LETTER

doi:10.1038/nature09696

Entanglement in a solid-state spin ensemble

Stephanie Simmons[1], Richard M. Brown[1], Helge Riemann[2], Nikolai V. Abrosimov[2], Peter Becker[3], Hans-Joachim Pohl[4], Mike L. W. Thewalt[5], Kohei M. Itoh[6] & John J. L. Morton[1,7]

Entanglement is the quintessential quantum phenomenon. It is a necessary ingredient in most emerging quantum technologies, including quantum repeaters[1], quantum information processing[2] and the strongest forms of quantum cryptography[3]. Spin ensembles, such as those used in liquid-state nuclear magnetic resonance[4,5], have been important for the development of quantum control methods. However, these demonstrations contain no entanglement and ultimately constitute classical simulations of quantum algorithms. Here we report the on-demand generation of entanglement between an ensemble of electron and nuclear spins in isotopically engineered, phosphorus-doped silicon. We combined high-field (3.4 T), low-temperature (2.9 K) electron spin resonance with hyperpolarization of the ^{31}P nuclear spin to obtain an initial state of sufficient purity to create a non-classical, inseparable state. The state was verified using density matrix tomography based on geometric phase gates, and had a fidelity of 98% relative to the ideal state at this field and temperature. The entanglement operation was performed simultaneously, with high fidelity, on 10^{10} spin pairs; this fulfils one of the essential requirements for a silicon-based quantum information processor.

Most quantum information processing algorithms applied to spin ensembles have been implemented in a regime of weak spin polarization. However, owing to the very low purity of the states used, any exponential enhancement offered by quantum mechanics disappears when the scaling of total resources is considered. Highly mixed, or weakly initialized, ensembles are often interpreted as the sum of a perfectly mixed component (given by a normalized identity matrix in the density matrix representation) and a small amount, ε, of a pure component, ρ_0; thus, $\rho_{\mathrm{true}} = (1-\varepsilon)\hat{\mathrm{I}}/d + \varepsilon\rho_0$, where d is the dimensionality of the state. The $\hat{\mathrm{I}}$ component is invariant under unitary operations and is not directly observable by magnetic resonance, which produces measurements of the population differences across allowed electron and nuclear spin transitions. It is therefore straightforward to ignore the maximally mixed component: this approach is called the 'pseudo-pure approximation'[6].

There are a number of entanglement witnesses or monotones that can distinguish entangled states from (classical) separable ones. A widely used test is the positive partial transpose (PPT) criterion, which is both a necessary and a sufficient test of entanglement for two coupled, spin-1/2 particles[7,8]. Applying this test to the mixed state above, ρ_{true}, it can be shown[8] that the minimum value of ε which permits the overall state to be entangled is 1/3.

Typical values for ε in liquid-state nuclear magnetic resonance and electron spin resonance (using 10-GHz excitation at a temperature of 5 K) are $\sim 10^{-5}$ and $\sim 10^{-2}$, respectively. These values are well below the required threshold for the PPT test. Thus, although experiments performed in this regime provide a valuable test bed for techniques in entanglement generation and detection[9], the states created are only pseudo-entangled, and are fully separable. (A notable exception was the use of chemical methods to generate highly polarized hydrogen spin pairs[10], though that is a single-shot experiment with limited scalability.) To overcome this limit, we require states of higher initial purity and a method to measure the $\hat{\mathrm{I}}$ component of the density matrix.

We follow a hybrid approach, using both the electron spin and the nuclear spin associated with a phosphorus donor in silicon. Isolated donors in isotopically engineered semiconductors are of particular interest as they possess excellent decoherence characteristics (both the electron and the nuclear coherence times, T_2, exceed seconds[11,12]), can be controlled with high fidelity using microwave and radio-frequency pulses[13,14], and are promising for integrating quantum technologies into conventional semiconductor devices[15].

Neglecting the weak polarization of the nuclear spin, the initial state populations are determined by the electron spin Zeeman energy, as shown in Fig. 1a, where $\alpha = \exp(-g\mu_{\mathrm{B}}B/k_{\mathrm{B}}T)$, g is the electron g-factor, μ_{B} is the Bohr magneton, k_{B} is Boltzmann's constant, and B and T are the experimental magnetic field and temperature, respectively. At a high magnetic field (3.4 T) and low temperature (2.9 K), the donor electron spin is thermally polarized to ~66%; however, the ^{31}P nuclear spin, with a much weaker magnetic moment, has only ~0.04% polarization. Various methods, collectively known as dynamic nuclear

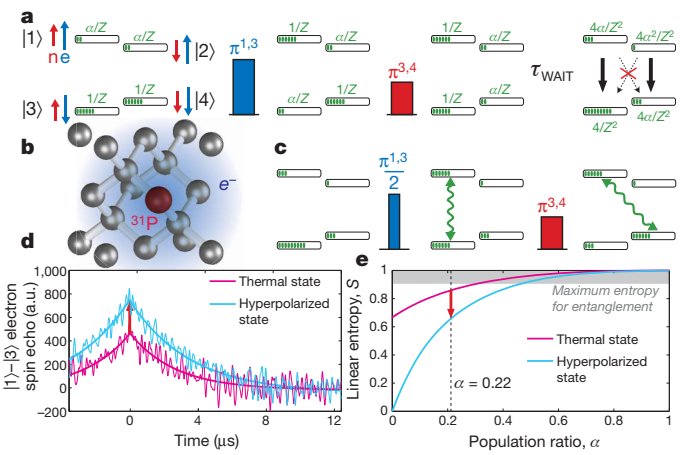

Figure 1 | Sequences for nuclear spin hyperpolarization and entanglement generation for this coupled $S = 1/2$, $I = 1/2$ spin system. a, The initial state is at thermal equilibrium, where populations (green) are distributed according to the electron spin (e) polarization at this magnetic field and temperature (see text). A pair of applied microwave and radio-frequency π pulses move spin populations to favour the $|\uparrow\rangle$ nuclear spin (n) state. After some time, $\tau_{\mathrm{WAIT}} \gg T_{1\mathrm{e}}$, there is a significant majority population in state $|3\rangle$, or $|\uparrow\downarrow\rangle$ (where the first and second arrows indicate the nuclear and electron spins, respectively). Nuclear spin and cross-relaxation processes occur on timescales much longer than $T_{1\mathrm{e}}$. **b**, Illustration of the ^{28}Si:P coupled spin system. **c**, Starting from the hyperpolarized state in **a**, an electron spin coherence is generated and transformed into the final entangled state, containing a superposition of $|\uparrow\uparrow\rangle$ and $|\downarrow\downarrow\rangle$. **d**, The growth in the electron spin echo intensity measured on the $|1\rangle$–$|3\rangle$ transition provides a measure of the population ratio, α. a.u., arbitrary units. **e**, This hyperpolarization sequence minimizes the linear entropy of the two-spin state for a given value of α.

[1]Department of Materials, Oxford University, Oxford OX1 3PH, UK. [2]Leibniz-Institut für Kristallzüchtung, 12489 Berlin, Germany. [3]PTB Braunschweig, 38116 Braunschweig, Germany. [4]VITCON Projectconsult GmbH, 07743 Jena, Germany. [5]Department of Physics, Simon Fraser University, Burnaby, British Columbia V5A 1S6, Canada. [6]School of Fundamental Science and Technology, Keio University, Yokohama, 3-14-1 Hiyoshi, 223-8522, Japan. [7]CAESR, Clarendon Laboratory, Oxford University, Oxford OX1 3PU, UK.

polarization[16,17], exist for indirectly transferring electron spin polarization to the nuclear spin and often exploit cross-relaxation processes involving simultaneous electron and nuclear spin flips. Here we exploit the relative absence of cross-relaxation leading to a substantial difference in the relaxation times of the electron and nuclear spins[13], to hyperpolarize the nuclear spin rapidly and with high efficiency. This hyperpolarization process is similar to 'algorithmic cooling' methods, whereby a particular quantum bit (qubit) relaxes quickly owing to coupling to a heat bath[18].

Figure 1 illustrates our method for tackling the twin challenges of measuring and minimizing the $\hat{\mathrm{I}}$ component in the density matrix of the coupled electron–nuclear spin system. The hyperpolarization of the nuclear spin can be understood as a SWAP operation (which interchanges the states of two qubits) with the (thermally polarized) electron spin, using a combination of resonant microwave and radio-frequency π pulses. This is followed by a delay τ_{WAIT}, which is substantially longer than the electron spin relaxation time, $T_{1\mathrm{e}}$ (specifically, $\tau_{\mathrm{WAIT}} \approx 8T_{1\mathrm{e}}$), during which the electron spin relaxes back to thermal equilibrium. On this timescale, other relaxation processes (such as pure nuclear spin flips or electron–nuclear spin flip-flops) are orders of magnitude slower and can be neglected. The resulting hyperpolarized state is

$$\rho = \frac{4}{Z^2}\left(\alpha|1\rangle\langle 1| + \alpha^2|2\rangle\langle 2| + |3\rangle\langle 3| + \alpha|4\rangle\langle 4|\right)$$

where $Z = 2(1+\alpha)$ is a normalizing constant.

Although spin echo sequences can only be used to probe the population differences across energy levels, we can obtain a direct measure of the population ratio, α, by measuring the electron spin echo amplitude between levels $|1\rangle$ and $|3\rangle$ before and after the hyperpolarization sequence, as shown in Fig. 1d. Owing to the enhanced polarization of the nuclear spin, a spin echo measured on this transition increases by a factor of $2/(\alpha+1)$ in comparison with the measurement from a fully relaxed thermal state. This measure is strictly conservative: it places a lower bound on the true polarization of the electron, as imperfections such as pulse errors or residual relaxation processes only lead to a lower apparent state purity. Using this measure, we observe an enhancement of the echo intensity by a factor of 1.643(2), corresponding to an upper bound of $\alpha \leq 0.217(2)$.

Linear spin entropy (defined as $\mathcal{N}[1-\mathrm{Tr}(\rho^2)]/(\mathcal{N}-1)$ for an $\mathcal{N}$-dimensional Hilbert space) is a useful characterization of a state's purity, and ranges from one, for maximally mixed states, to zero, for pure states. Our hyperpolarization sequence corresponds to a decrease in linear spin entropy, made possible by the open quantum system's contact with the lattice heat bath (Fig. 1e). Importantly, this approach leads to the minimum possible linear entropy given the electron spin polarization resource and type of relaxation present[18]. Entanglement is maximized in a mixed, two-qubit density matrix by first minimizing the linear entropy and then generating an entangled coherence across the levels with the largest and second-smallest populations[19,20]. Following this strategy, we create an entangled state using a coherence-generating microwave $\pi^{1,3}/2$ pulse (where the superscript denotes the pair of levels addressed by the pulse) followed by a radio-frequency $\pi^{3,4}$ pulse (Fig. 1c), yielding the target state:

$$\rho = \frac{1}{2Z^2}\begin{pmatrix} 1+\alpha & 0 & 0 & 1-\alpha \\ 0 & 2\alpha^2 & 0 & 0 \\ 0 & 0 & 2\alpha & 0 \\ 1-\alpha & 0 & 0 & 1+\alpha \end{pmatrix}$$

This density matrix is entangled according to the PPT criterion when $\alpha \leq 0.432$; other preparation methods (such as pseudo-pure state preparation) require substantially higher polarization (Supplementary Information).

Having prepared the initial state and performed an entangling operation, we now use density matrix tomography to extract the final two-spin state. Owing to the weak magnetic moment of nuclear spins and necessarily low donor concentration in our sample, we are restricted to non-projective measurements of the electron spin ensemble along the σ_x and σ_y Pauli bases, which can be performed selectively on the m_I state of the nuclear spin (in product operator formalism, these bases can be written as $S_{x,y}I^{\alpha,\beta}$).

Diagonal elements of the density matrix (corresponding to state populations) are obtained by mapping pairs of population differences into an electron spin echo on the $|1\rangle$–$|3\rangle$ transition ($S_{x,y}I^{\alpha}$). The accurate detection of off-diagonal elements (coherences) is a more elaborate process, made by selectively labelling the coherence between each pair of eigenstates with a distinguishable, time-varying phase[9]. By this process, a particular phase accumulation rate provides the signature of a particular coherence, allowing the off-diagonal elements to be reconstructed from the amplitudes in the Fourier transform of a measured signal.

Here we follow an approach inspired by the Aharonov–Anandan geometric phase gate[21,22] to apply arbitrary phases in a fixed time to the four different eigenstates, and thus separately label each of the possible coherences. We apply two π pulses, along different axes, across a transition between a pair of eigenstates. The phase acquired by each eigenstate is opposite and equal to half the solid angle of its trajectory on the Bloch sphere (Fig. 2a). Thus, applying $\pi_0^{1,3}$ followed by $-\pi_\phi^{1,3}$ (subscripts denote pulse phase and, thus, nominal rotation axis) leads eigenstates $|1\rangle$ and $|3\rangle$ to assume trajectories of equal and opposite solid angle, $\pm 2\phi$. A similar operation, $\pi_0^{3,4}$ followed by $-\pi_\sigma^{3,4}$, is applied to the nuclear spin transition, such that the total operator describing the action of these four pulses is

$$U(\phi,\sigma) = \begin{pmatrix} \mathrm{e}^{-i\phi} & 0 & 0 & 0 \\ 0 & 1 & 0 & 0 \\ 0 & 0 & \mathrm{e}^{i(\sigma+\phi)} & 0 \\ 0 & 0 & 0 & \mathrm{e}^{-i\sigma} \end{pmatrix}$$

The value of ϕ is incremented by $\delta\phi$ on each shot of the experiment, with effective frequency $\nu_\phi = 2\pi/\delta\phi$ (and similarly for σ, $\delta\sigma$ and ν_σ). We then map each off-diagonal element of the density matrix in turn into $S_{x,y}I^{\alpha}$ using a set of appropriate microwave and radio-frequency π

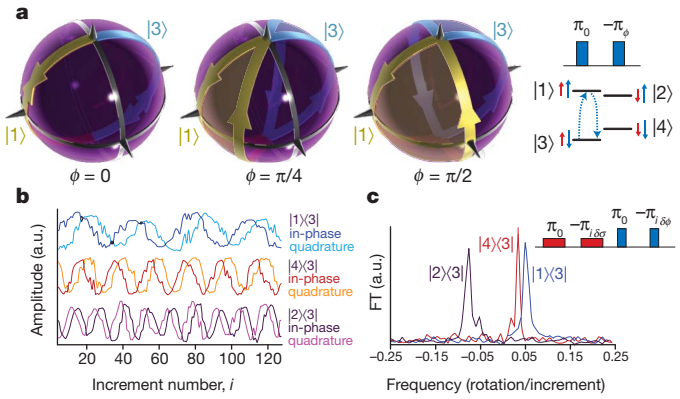

Figure 2 | Electron and nuclear spin phase rotations reveal the off-diagonal elements of the density matrix. **a**, Under the application of two consecutive $\pi^{1,3}$ pulses around different axes (ϕ), the eigenstates $|1\rangle$ and $|3\rangle$ undergo closed trajectories on the Bloch sphere with equal and opposite solid angles, $\Omega = \pm 2\phi$. Each state picks up a phase equal to half this solid angle. **b**, This π_0, $-\pi_\phi$ phase gate is applied to both electron $|1\rangle$–$|3\rangle$ and nuclear $|3\rangle$–$|4\rangle$ transitions, where the two phases are varied by different increments, $\delta\phi$ and $\delta\sigma$, as the experiment is repeated. Example oscillations are shown for three experiments where we generate an electron coherence, $|1\rangle\langle 3|$, a nuclear coherence, $|4\rangle\langle 3|$ and a zero quantum coherence, $|2\rangle\langle 3|$. **c**, Fourier transforms (FT) of the oscillations with respect to increment number show peaks located at the frequencies 0.050(8), 0.031(5) and −0.079(8), in agreement with the frequencies that were set, $\nu_\phi = 2\pi/\delta\phi = 0.05$ and $\nu_\sigma = 2\pi/\delta\sigma = 0.03$.

pulses, and measure the amplitude of the Fourier component at the effective frequency corresponding to that coherence. Quadrature measurement allows us to discriminate between positive and negative frequencies. The presence of other Fourier peaks would be illustrative of pulse errors in the mapping sequence, but as seen in Fig. 2b, c, such errors are negligible even in the absence of operations such as phase cycling.

By combining our measurements of the identity component and the diagonal and off-diagonal elements of the density matrix of the electron-nuclear spin system, we obtain the following expression for ρ:

$$\begin{pmatrix} 0.382 & 0.003+0.000i & -0.035-0.039i & 0.272 \\ 0.003-0.000i & 0.017 & -0.000+0.001i & 0.001+0.003i \\ -0.035+0.039i & -0.000-0.001i & 0.174 & -0.055-0.042i \\ 0.272 & 0.001-0.003i & -0.055+0.042i & 0.427 \end{pmatrix}$$

This state has a minimum eigenvalue under the PPT test of $-0.19(1)$ and a concurrence, C, of 0.43(4), each of which confirms the presence of finite entanglement. The results of this tomography process are shown in Fig. 3. The fidelity of the measured density matrix with respect to the target state, given that $\alpha = 0.217$, is 98.2(2)%, and is 68(2)% with respect to an ideal Bell state ($\alpha = 0$). To obtain the uncertainty in these values, we used Monte Carlo generation of physical density matrices based on the standard error of each matrix element due to noise (Supplementary Information).

The finite entanglement shown can offer direct advantages over classical methods in applications such as quantum sensors[23]. To achieve higher-purity entangled states, we could use lower temperatures; for example, we would expect $C \approx 0.99$ if these experiments were performed at 0.8 K. Complementary to this approach, entanglement purification could be performed using a larger Hilbert space at each node[24], for example using a donor atom with a higher nuclear spin (such as bismuth, with $I = 9/2$).

The electron–nuclear spin entanglement generated here could also be mapped into an entangled state between nuclear spin pairs[25]. By interchanging (by SWAP) the state of the electron spin with a second, coupled nucleus, for example, nuclear spin entanglement could be attained in a regime where the thermal polarization of the nuclei would be orders of magnitude too small and the direct coupling between them weak. Clusters of up to eight nuclei coupled to a single electron spin have been explored in other materials[26], although the scaling of such an approach seems limited. A scalable network of entangled nuclear spins could be generated by exploiting the ability to ionize the donor and transfer the electron onto a neighbouring donor site[27,28]. These operations, combined with single-shot read-out of the phosphorus donor spin[29] and globally controlled electron–nuclear spin entanglement such as we have demonstrated, form the basis for a cluster-state quantum computer in silicon[25].

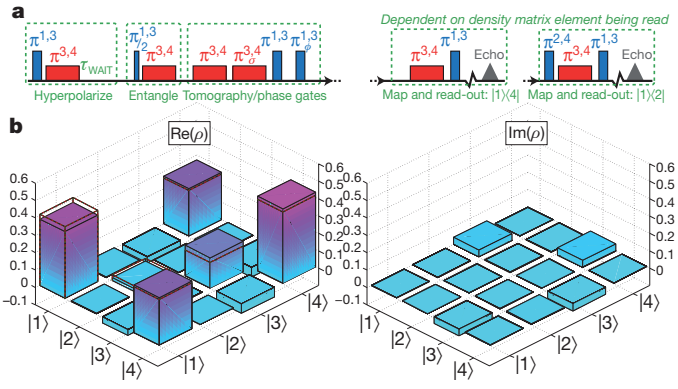

Figure 3 | Measuring an entangled density matrix. a, The full pulse sequence used to prepare, entangle and measure the two-spin state. The final read-out stage was changed according to the density matrix element being measured: examples are shown for the $|1\rangle\langle 2|$ and $|1\rangle\langle 4|$ states. **b**, The obtained density matrix is shown as solid bars, and the dashed outline (zero where not shown) shows that of an ideal state given $\alpha = 0.217$. The fidelity of the ideal state with the measured density matrix is 98%.

METHODS SUMMARY

Si:P consists of an electron spin, $S = 1/2$ ($g = 1.9987$), coupled to the nuclear spin, $I = 1/2$, of ^{31}P through an isotropic hyperfine coupling of $a = 4.19$ mT. The W-band electron spin resonance signal comprises two lines (one for each nuclear spin projection, $M_I = \pm 1/2$). Our experiments were performed on the low-field line of the electron spin resonance doublet, corresponding to $M_I = 1/2$. At 2.9 K and 3.36 T, the electron and nuclear spin relaxation times were measured to be approximately 0.6 s and 100 s, respectively.

The sample consists of a ^{28}Si-enriched single crystal about 0.5 mm in diameter with a residual ^{29}Si concentration of order 70 p.p.m., produced by decomposing isotopically enriched silane in a recirculating reactor to produce poly-silicon rods, followed by floating-zone crystallization. Phosphorus doping of $\sim 10^{14}$ cm^{-3} was achieved by adding dilute PH_3 gas to the ambient argon during the final floating-zone single-crystal growth. Further information on the sample growth has been reported elsewhere[30].

Pulsed electron spin resonance experiments were performed using a W-band (94-GHz) Bruker ELEXSYS 680 spectrometer, modified to allow microwave phase control and equipped with a 6-T superconducting magnet and a low-temperature helium-flow cryostat (Oxford CF935). The cryostat was pumped to achieve a temperature of 2.88 K (internal thermocouple) consistent with the spin temperature measurement (see text). Typical pulse times were 56 ns for a microwave π pulse and 100 μs for a radio-frequency π pulse. To achieve arbitrary phase control, we generated radio-frequency pulses using a Rohde and Schwarz AFQ100B together with an Amplifier Research 500 W amplifier.

Received 30 September; accepted 23 November 2010.
Published online 19 January 2011.

1. Briegel, H.-J., Dür, W., Cirac, J. I. & Zoller, P. Quantum repeaters: the role of imperfect local operations in quantum communication. *Phys. Rev. Lett.* **81,** 5932–5935 (1998).
2. Jozsa, R. & Linden, N. On the role of entanglement in quantum-computational speed-up. *Proc. R. Soc. Lond. A* **459,** 2011–2032 (2003).
3. Curty, M., Lewenstein, M. & Lütkenhaus, N. Entanglement as a precondition for secure quantum key distribution. *Phys. Rev. Lett.* **92,** 217903 (2004).
4. Vandersypen, L. *et al.* Experimental realization of Shor's quantum factoring algorithm using nuclear magnetic resonance. *Nature* **414,** 883–887 (2001).
5. Negrevergne, C. *et al.* Benchmarking quantum control methods on a 12-qubit system. *Phys. Rev. Lett.* **96,** 170501 (2006).
6. Knill, E., Chuang, I. & Laflamme, R. Effective pure states for bulk quantum computation. *Phys. Rev. A* **57,** 3348–3363 (1998).
7. Horodecki, M., Horodecki, P. & Horodecki, R. Separability of mixed states: necessary and sufficient conditions. *Phys. Lett. A* **223,** 1–8 (1996).
8. Peres, A. Separability criterion for density matrices. *Phys. Rev. Lett.* **77,** 1413–1415 (1996).
9. Mehring, M., Mende, J. & Scherer, W. Entanglement between an electron and a nuclear spin 1/2. *Phys. Rev. Lett.* **90,** 153001 (2003).
10. Anwar, M. *et al.* Preparing high purity initial states for nuclear magnetic resonance quantum computing. *Phys. Rev. Lett.* **93,** 040501 (2004).
11. Morton, J. J. L. *et al.* Solid-state quantum memory using the ^{31}P nuclear spin. *Nature* **455,** 1085–1088 (2008).
12. Tyryshkin, A. M. & Lyon, S. A. Data presented at the Silicon Qubit Workshop, 23-24 August (Albuquerque, sponsored by Lawrence Berkeley National Laboratory and Sandia National Laboratory, 2010).
13. Tyryshkin, A. M. *et al.* Coherence of spin qubits in silicon. *J. Phys. Condens. Matter* **18,** S783–S794 (2006).
14. Morton, J. J. L. *et al.* High fidelity single qubit operations using pulsed electron paramagnetic resonance. *Phys. Rev. Lett.* **95,** 200501 (2005).
15. Kane, B. E. A silicon-based nuclear spin quantum computer. *Nature* **393,** 133–137 (1998).
16. Wollan, D. S. Dynamic nuclear polarization with an inhomogeneously broadened ESR line. II. Experiment. *Phys. Rev. B* **13,** 3686–3696 (1976).
17. Hayashi, H., Itahashi, T., Itoh, K. M., Vlasenko, L. S. & Vlasenko, M. P. Dynamic nuclear polarization of ^{29}Si nuclei in isotopically controlled phosphorus doped silicon. *Phys. Rev. B* **80,** 045201 (2009).
18. Schulman, L., Mor, T. & Weinstein, Y. Physical limits of heat-bath algorithmic cooling. *Phys. Rev. Lett.* **94,** 120501 (2005).
19. Wei, T. *et al.* Maximal entanglement versus entropy for mixed quantum states. *Phys. Rev. A* **67,** 022110 (2003).
20. Verstraete, F., Audenaert, K. & De Moor, B. Maximally entangled mixed states of two qubits. *Phys. Rev. A* **64,** 012316 (2001).
21. Aharonov, Y. & Anandan, J. Phase change during a cyclic quantum evolution. *Phys. Rev. Lett.* **58,** 1593–1596 (1987).
22. Suter, D., Mueller, K. T. & Pines, A. Study of the Aharonov-Anandan quantum phase by NMR interferometry. *Phys. Rev. Lett.* **60,** 1218–1220 (1988).

23. Simmons, S., Jones, J. A., Karlen, S. D., Ardavan, A. & Morton, J. J. L. Magnetic field sensors using 13-spin cat states. *Phys. Rev. A* **82,** 022330 (2010).
24. Campbell, E. T. Distributed quantum-information processing with minimal local resources. *Phys. Rev. A* **76,** 040302 (2007).
25. Morton, J. J. L. A silicon-based cluster state quantum computer. Preprint at ⟨http://128.84.158.119/abs/0905.4008v1⟩ (2009).
26. Mehring, M. & Mende, J. Spin-bus concept of spin quantum computing. *Phys. Rev. A* **73,** 052303 (2006).
27. Skinner, A., Davenport, M. & Kane, B. Hydrogenic spin quantum computing in silicon: a digital approach. *Phys. Rev. Lett.* **90,** 087901 (2003).
28. Andresen, S. *et al.* Charge state control and relaxation in an atomically doped silicon device. *Nano Lett.* **7,** 2000–2003 (2007).
29. Morello, A. *et al.* Single-shot readout of an electron spin in silicon. *Nature* **467,** 687–691 (2010).
30. Becker, P., Pohl, H.-J., Riemann, H. & Abrosimov, N. Enrichment of silicon for a better kilogram. *Phys. Status Solidi. A* **207,** 49–66 (2009).

Supplementary Information is linked to the online version of the paper at www.nature.com/nature.

Acknowledgements We thank J. Fitzsimons, S. Benjamin, A. Ardavan, A. Briggs and B. Lovett for discussions, and P. Höfer and Bruker BioSpin for support with instrumentation. Three-dimensional images were created using POV-RAY open-source software. We thank EPSRC for supporting work at Oxford through CAESR (EP/D048559/1) and the Oxford–Keio collaboration through the JST-EPSRC SIC programme (EP/H025952/1). Work at Keio has been supported by Grants-in-aid for Scientific Research by MEXT, FIRST by JSPS, Nanoquine and Keio GCOE. S.S. is supported by the Clarendon Fund, J.J.L.M. is supported by St John's College, Oxford, and the Royal Society.

Author Contributions S.S., R.M.B. and J.J.L.M. designed and performed the experiments and wrote the paper. H.R., N.V.A., P.B. and H.-J.P. grew the ^{28}Si crystal. K.M.I and M.L.W.T. analysed and prepared the sample and discussed the experiments, results and manuscript.

Author Information Reprints and permissions information is available at www.nature.com/reprints. The authors declare no competing financial interests. Readers are welcome to comment on the online version of this article at www.nature.com/nature. Correspondence and requests for materials should be addressed to J.J.L.M. (john.morton@materials.ox.ac.uk).